J. Fluid Mech. (2001), *vol.* 441, *pp.* 195–221. Printed in the United Kingdom

© 2001 Cambridge University Press

Thermocapillary effects on a thin viscous rivulet draining steadily down a uniformly heated or cooled slowly varying substrate

By D. HOLLAND, B. R. DUFFY AND S. K. WILSON

Department of Mathematics, University of Strathclyde, Livingstone Tower,
26 Richmond Street, Glasgow G1 1XH, UK
e-mail b.r.duffy@strath.ac.uk; s.k.wilson@strath.ac.uk

(Received 25 August 2000 and in revised form 16 February 2001)

We use the lubrication approximation to investigate the steady flow of a thin rivulet of viscous fluid with prescribed volume flux draining down a planar or slowly varying substrate that is either uniformly hotter or uniformly colder than the surrounding atmosphere, when the surface tension of the fluid varies linearly with temperature. Utilizing the (implicit) solution of the governing ordinary differential equation that emerges, we undertake a comprehensive asymptotic and numerical analysis of the flow. In particular it is shown that the variation in surface tension drives a transverse flow that causes the fluid particles to spiral down the rivulet in helical vortices (which are absent in the corresponding isothermal problem). We find that a single continuous rivulet can run from the top to the bottom of a large horizontal circular cylinder provided that the cylinder is either warmer or significantly cooler than the surrounding atmosphere, but if it is only slightly cooler then a continuous rivulet is possible only for a sufficiently small flux (though a rivulet with a discontinuity in the free surface is possible for larger values of the flux). Moreover, near the top of the cylinder the rivulet has finite depth but infinite width, whereas near the bottom of the cylinder it has finite width and infinite depth if the cylinder is heated or slightly cooled, but has infinite width and finite depth if the cylinder is significantly cooled.

1. Introduction

The gravity-driven draining of a rivulet of a viscous fluid down an inclined substrate is a fundamental model problem for a number of practical situations, including a variety of geophysical flows and industrial devices such as condensers and heat exchangers, and has been the subject of considerable theoretical and experimental interest both in its own right and as a prototype problem for a much wider class of flows with contact lines.

The steady unidirectional flow of a uniform rivulet of Newtonian fluid down an inclined plane was studied by Towell & Rothfeld (1966), who calculated the profile of the rivulet numerically and found excellent agreement with their own experimental results. More recently Alekseenko, Geshev & Kuibin (1997) extended Towell & Rothfeld's (1966) approach in a numerical study of the flow of a uniform rivulet along the underside of an inclined cylinder.

Allen & Biggin (1974) and Duffy & Moffatt (1995) used the lubrication approximation to obtain an analytical solution for the flow of a uniform rivulet down an

https://doi.org/10.1017/S0022112001004797 Published online by Cambridge University Press

inclined plane in the case when the cross-sectional profile of the rivulet transverse to the direction of flow is slender. In particular, Duffy & Moffatt (1995) calculated the profile of the rivulet as a function of the angle of inclination of the plane to the horizontal and used this locally unidirectional solution to investigate the flow of a non-uniform rivulet down a slowly varying substrate, specifically flow in the azimuthal direction round a large horizontal cylinder. Kuibin (1996) studied the flow of a thin uniform rivulet along the underside of an inclined cylinder. Wilson & Duffy (1998) studied the flow of a non-uniform rivulet down a slowly varying substrate with variation transverse to the direction of flow, specifically flow in the azimuthal direction round a large horizontal cylinder with a ridge or trough in the azimuthal direction. Rosenblat (1983) investigated the flow of a uniform rivulet of viscoelastic fluid down an inclined plane and found that one effect of the elasticity is to drive a transverse flow (absent in the Newtonian case) which causes the fluid particles to spiral down the rivulet in two counter-rotating helical vortices.

Various aspects of the stability of rivulet flow have been investigated by, for example, Davis (1980), Weiland & Davis (1981), Young & Davis (1987), Schmuki & Laso (1990), and Wilson & Duffy (1998).

Taking a slightly different approach Smith (1973) obtained a similarity solution of the thin-film equations describing the steady gravity-driven draining of a slender non-uniform rivulet from a point source on an inclined plane in the absence of surface-tension effects. In particular, Smith's (1973) solution predicts that the width of the rivulet increases according to the 3/7th power of the distance measured down the plane from the source, and is in excellent agreement with his own experimental results. Subsequently Duffy & Moffatt (1997) obtained the corresponding solution when surface-tension effects are dominant (as they are, for example, when the plane is vertical) and found that Smith's (1973) exponent is modified to a 3/13th power. Both of these similarity solutions predict a varying contact angle at the contact line; Wilson, Duffy & Davis (2001) showed how they can be modified to accommodate a fixed-contact-angle condition at the contact line if sufficiently strong slip at the solid/fluid interface is incorporated into the model.

There has also been considerable work on the closely related problem of the formation and stability of a dry patch in a thin film draining under gravity down an inclined plane (see, for example, Hartley & Murgatroyd 1964; Ponter *et al.* 1967; Wilson 1974; Podgorski, Flesselles & Limat 1999; and Wilson *et al.* 2001).

All of the work on rivulets described thus far has concentrated on the simplest case of isothermal flow. However, in many practical and industrial contexts heating or cooling effects are not negligible, and so there is considerable interest in investigating the flow of non-isothermal rivulets. The pioneering work on non-isothermal thin-film flow was performed by Burelbach, Bankoff & Davis (1988) who formulated and analysed the general evolution equation for a two-dimensional thin film of fluid on a uniformly heated or cooled horizontal plane, including the effects of mass loss or gain, vapour recoil, thermocapillarity, surface tension, gravity and long-range intermolecular attraction. Ehrhard & Davis (1991) used a special case of this equation (and the corresponding equation for axisymmetric flow) to study the non-isothermal quasi-static spreading of both two-dimensional and axisymmetric droplets on a uniformly heated or cooled horizontal plane subject to thermocapillary effects. In the absence of exact solutions of the relevant governing equations for the profiles of the droplets their analytical (as opposed to numerical) analysis of the non-isothermal problem was largely restricted to the case of weak thermocapillary effects. Subsequently Ehrhard (1993) conducted a series of experiments on both isothermal and non-isothermal

https://doi.org/10.1017/S0022112001004797 Published online by Cambridge University Press

spreading, and found good agreement with the theoretical predictions of Ehrhard & Davis (1991). Also of relevance to the present work are other studies of non-isothermal thin-film flows with thermocapillary effects, notably the following papers: Tan, Bankoff & Davis (1990) and Burelbach, Bankoff & Davis (1990) on the steady thermocapillary-driven flow on a non-uniformly heated horizontal plane; Reisfeld & Bankoff (1992) on the flow round a heated or cooled horizontal cylinder; Jensen & Grotberg (1993) on the surface-tension-gradient-driven spreading of heat or soluble surfactant along a thin film; Anderson & Davis (1995) on the spreading of a volatile droplet on a heated horizontal plane; Braun *et al.* (1995) on the spreading of a reacting droplet on a heated horizontal plane; Smith (1995) on the thermocapillary-driven motion of a droplet on a non-uniformly heated horizontal plane; Joo, Davis & Bankoff (1996) on the mechanism for rivulet formation in a thin film draining down a heated inclined plane; López, Bankoff & Miksis (1996) on the advancing contact line at the leading edge of a film draining down a heated inclined plane; and Kataoka & Troian (1997, 1998) on the advancing contact line at the leading edge of a thermocapillary-driven film on a non-uniformly heated vertical plane. The review article by Oron, Davis & Bankoff (1997) gives an excellent overview of recent work on both isothermal and non-isothermal thin-film flows. There has also been considerable work on the onset of thermocapillary-driven (Marangoni) convection in fluid layers. Davis (1987) reviews the early work in this area.

In this paper we shall employ the approach adopted by Duffy & Moffatt (1995) for the isothermal problem and use the lubrication approximation to investigate the steady flow of a thin rivulet of viscous fluid with prescribed volume flux draining down a planar or slowly varying substrate that is either uniformly hotter or uniformly colder than the surrounding atmosphere, when the surface tension of the fluid varies linearly with temperature. In the course of this work we shall obtain the (implicit) solution of the ordinary differential equation for the free-surface profile of the rivulet that arises, and as a result we are able to analyse the behaviour of the rivulet for arbitrarily strong thermocapillary effects.

2. Formulation

Consider the steady flow of a symmetric rivulet (of uniform width $2a$ and prescribed volume flux Q) of an incompressible Newtonian fluid with uniform density ρ, viscosity μ, specific heat c and thermal conductivity $k_{\rm th}$ down a planar substrate inclined at an angle α ($0 < \alpha < \pi$) to the horizontal. The velocity $\boldsymbol{u} = (u, v, w)$, pressure p, and temperature T of the fluid are governed by the mass conservation, Navier–Stokes and energy equations

$$\nabla \cdot \boldsymbol{u} = 0, \tag{1}$$

$$\rho(\boldsymbol{u} \cdot \nabla)\boldsymbol{u} = -\nabla p + \mu \nabla^2 \boldsymbol{u} + \rho \boldsymbol{g}, \tag{2}$$

$$\rho c(\boldsymbol{u} \cdot \nabla)T = k_{\rm th} \nabla^2 T, \tag{3}$$

where $\boldsymbol{g} = g(\sin\alpha, 0, -\cos\alpha)$ is the acceleration due to gravity, referred to the Cartesian coordinates $Oxyz$ indicated in figure 1. At the solid substrate $z = 0$ the fluid velocity is zero and the uniform temperature is prescribed:

$$\boldsymbol{u} = \boldsymbol{0}, \qquad T = T_0; \tag{4}$$

on the free surface $z = h(x, y)$ the appropriate boundary conditions are normal and tangential stress balances, an energy balance and the kinematic condition, which take

https://doi.org/10.1017/S0022112001004797 Published online by Cambridge University Press

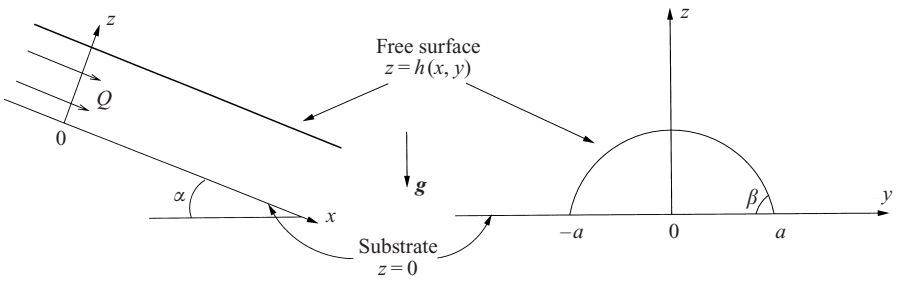


FIGURE 1. Geometry of the problem.

the form

$$\boldsymbol{n}\cdot\boldsymbol{T}\cdot\boldsymbol{n} = -\gamma\kappa, \tag{5}$$

$$\boldsymbol{t}\cdot\boldsymbol{T}\cdot\boldsymbol{n} = \boldsymbol{t}\cdot\nabla\gamma, \tag{6}$$

$$-k_{\mathrm{th}}\nabla T\cdot\boldsymbol{n} = \alpha_{\mathrm{th}}(T - T_\infty), \tag{7}$$

$$uh_x + vh_y = w. \tag{8}$$

Here $\boldsymbol{T}$ denotes the stress tensor of the fluid, $\boldsymbol{n}$ and $\boldsymbol{t}$ are unit normal and tangential vectors to the free surface, T_0 is the prescribed uniform temperature of the plate, T_∞ is the prescribed uniform temperature of the passive atmosphere above the rivulet, γ is the surface tension, α_{th} is the surface heat-transfer coefficient, κ is twice the mean curvature of the free surface, and suffixes x and y denote derivatives. We take μ, ρ, c, k_{th} and α_{th} to be constants, but we assume that the surface tension γ depends linearly on temperature:

$$\gamma(T) = \gamma_0 - \lambda(T - T_0), \tag{9}$$

where $\lambda = -\mathrm{d}\gamma/\mathrm{d}T$ is a positive constant and γ_0 is the constant surface tension at $T = T_0$. The kinematic condition (8) may conveniently be rewritten in the form

$$\bar{u}_x + \bar{v}_y = 0, \tag{10}$$

where the local fluxes $\bar{u}$ and $\bar{v}$ are defined as

$$\bar{u} = \int_0^h u\,\mathrm{d}z, \quad \bar{v} = \int_0^h v\,\mathrm{d}z. \tag{11}$$

At the edges of the rivulet $y = \pm a$ where $h = 0$ we assume that the contact angle takes the prescribed constant value β, as shown in figure 1. The prescribed volume flux of fluid down the substrate is given by

$$Q = \int_{-a}^{a}\int_0^h u\,\mathrm{d}z\,\mathrm{d}y. \tag{12}$$

Unlike the corresponding isothermal problem studied by Duffy & Moffatt (1995), the present problem has no rectilinear-flow solution, since the imposed temperature difference between the substrate and the surrounding atmosphere leads to a surface-tension variation at the free surface of the fluid that inevitably drives a transverse flow (in addition to the gravity-driven longitudinal flow down the substrate), and so the flow is fully three-dimensional. We continue by considering a solution in which all quantities are independent of x, so that, in particular, $h = h(y)$. Moreover we shall consider only solutions that are symmetric about $y = 0$ and smooth at $y = 0$, so that

https://doi.org/10.1017/S0022112001004797 Published online by Cambridge University Press

they satisfy

$$h_y = 0, \quad h_{yyy} = 0 \tag{13}$$

at $y = 0$; therefore hereafter we need consider the solution in $0 \leqslant y \leqslant a$ only (with the behaviour in $-a \leqslant y \leqslant 0$ given by symmetry).

Equations (1)–(13) constitute a formidable problem on which little progress can be made analytically in general; however, considerable progress can be made in the case of a rivulet whose cross-section is slender (with, in particular, $\beta \ll 1$), and it is this case that we consider from now on. We scale the system as follows:

$$\left.\begin{aligned} &y = ly^*, \quad z = \beta l z^*, \quad a = la^*, \quad h = \beta l h^*, \\ &u = \frac{\rho g \beta^2 l^2}{\mu} u^*, \quad v = \frac{\rho g \beta^3 l^2}{\mu} v^*, \quad w = \frac{\rho g \beta^4 l^2}{\mu} w^*, \quad p = \rho g \beta l p^*, \\ &Q = \frac{\rho g \beta^3 l^4}{\mu} Q^*, \quad \gamma = \gamma_0 \gamma^*, \quad T = T_\infty + (T_0 - T_\infty) T^*, \end{aligned}\right\} \tag{14}$$

where $l = (\gamma_0/\rho g)^{1/2}$ is the capillary length. Then with superscript stars dropped, the scaled governing equations at leading order in β are

$$v_y + w_z = 0, \tag{15}$$

$$0 = \sin\alpha + u_{zz}, \tag{16}$$

$$0 = -p_y + v_{zz}, \tag{17}$$

$$0 = -p_z - \cos\alpha, \tag{18}$$

$$T_{zz} = 0, \tag{19}$$

$$\bar{v}_y = 0, \tag{20}$$

with the boundary conditions

$$u = v = w = 0, \quad T = 1 \tag{21}$$

on $z = 0$,

$$-p = h_{yy}, \tag{22}$$

$$u_z = 0, \tag{23}$$

$$v_z = -\frac{1}{\Delta C}(T_y + h_y T_z), \tag{24}$$

$$T_z + BT = 0 \tag{25}$$

on $z = h$,

$$h = 0, \quad h_y = -1 \tag{26}$$

at $y = a$, and (13) at $y = 0$, where the non-dimensional thermocapillary number ΔC and Biot number B are defined as

$$\Delta C = \frac{\rho g \beta^2 l^2}{\lambda(T_0 - T_\infty)}, \quad B = \frac{\beta l \alpha_{\text{th}}}{k_{\text{th}}}. \tag{27}$$

Solving (18) subject to (22) on $z = h$ we obtain

$$p = (h - z)\cos\alpha - h_{yy}, \tag{28}$$

https://doi.org/10.1017/S0022112001004797 Published online by Cambridge University Press

and solving (19) subject to the thermal boundary conditions (21) on $z = 0$ and (25) on $z = h$ gives

$$T = 1 - \frac{Bz}{1 + Bh}. \tag{29}$$

The velocity is then found from (15)–(17), (21) on $z = 0$, and (23) and (24) on $z = h$ to be

$$u = \tfrac{1}{2}z(2h - z)\sin\alpha, \tag{30}$$

$$v = -\frac{p_y}{2}z(2h - z) + \frac{Mh_y z}{(1 + Bh)^2}, \tag{31}$$

$$w = \frac{p_{yy}}{6}z^2(3h - z) + \frac{p_y}{2}h_y z^2 - \frac{Mz^2}{2(1 + Bh)^2}\left(h_{yy} - \frac{2Bh_y^2}{1 + Bh}\right), \tag{32}$$

where M is an effective Marangoni number defined by

$$M = \frac{B}{\Delta C} = \frac{\lambda\alpha_{\mathrm{th}}(T_0 - T_\infty)}{\rho g\beta l k_{\mathrm{th}}}, \tag{33}$$

so that $M > 0$ (< 0) when the substrate is hotter (colder) than the surrounding atmosphere. Substituting (30) into (12) gives the volume flux

$$Q = \frac{\sin\alpha}{3}\int_{-a}^{a} h^3\,\mathrm{d}y. \tag{34}$$

From the kinematic condition (20) we obtain

$$\left[-\frac{p_y h^3}{3} + \frac{Mh^2 h_y}{2(1 + Bh)^2}\right]_y = 0, \tag{35}$$

and substituting for p from (28), integrating once with respect to y and then using the conditions (13) we obtain a third-order ordinary differential equation for h, namely

$$(h_{yy} - h\cos\alpha)_y + \frac{3Mh_y}{2h(1 + Bh)^2} = 0. \tag{36}$$

In the limit $B \to 0$ this becomes

$$(h_{yy} - h\cos\alpha)_y + \frac{3Mh_y}{2h} = 0, \tag{37}$$

which is of the same form as equation (5.5p) of Ehrhard & Davis (1991), derived by them to describe the profile of a two-dimensional drop of fluid of prescribed area that is spreading quasi-statically. We note from (36) or (37) and the boundary condition (26) that for $M \neq 0$ the curvature of the free surface at the contact line $y = a$ is singular (with $h_{yy} \sim -\frac{3}{2}M\log h$ as $h \to 0$), and that

$$h \sim (a - y) - \tfrac{3}{4}M(a - y)^2\log(a - y) \tag{38}$$

as $y \to a$.

The discussion thus far has been restricted to flow down a planar substrate, but as Duffy & Moffatt (1995) describe, the analysis also provides the leading-order approximation to the local behaviour of a rivulet of non-uniform width draining down a non-planar cylindrical substrate (with horizontal generators), with α now representing the local inclination of the substrate to the horizontal, provided that α varies sufficiently slowly (specifically, provided that the curvatures of the substrate

https://doi.org/10.1017/S0022112001004797 Published online by Cambridge University Press

and the rivulet profile in the downstream direction are much less than the transverse curvature of the rivulet). Thus results derived in subsequent sections may be interpreted as describing, for example, a slowly varying rivulet draining azimuthally from the top ($\alpha = 0$) to the bottom ($\alpha = \pi$) of a large horizontal circular cylinder. It is known (Wilson & Duffy 1998) that in the isothermal case $M = 0$ there are multiple branches of solutions in $\frac{1}{2}\pi < \alpha \leqslant \pi$, but that of these only the one that connects smoothly with the solution in $0 \leqslant \alpha < \frac{1}{2}\pi$ is physically realizable; we shall henceforth concern ourselves with only the latter type of solution.

3. An implicit solution and its properties

Integrating (36) twice with respect to y we find

$$h_y^2 - h^2\cos\alpha + 3Mh\left[\log\left(\frac{h}{1+Bh}\right) - 1\right] = Ch + D, \tag{39}$$

where C and D are constants of integration. Imposing the boundary condition (13a) in the form

$$h_y = 0 \text{ when } h = h_m, \tag{40}$$

where $h_m = h(0)$ denotes the (unknown) height at $y = 0$, and boundary conditions (26) in the form

$$h_y = -1 \text{ when } h = 0, \tag{41}$$

we obtain

$$h_y^2 = f(h), \tag{42}$$

where we have defined

$$f(h) = \left(1 - \frac{h}{h_m}\right)(1 - hh_m\cos\alpha) - 3Mh\log\left(\frac{h(1+Bh_m)}{h_m(1+Bh)}\right), \tag{43}$$

which must be non-negative in a physically relevant interval containing $h = 0$ and $h = h_m$. We show in Appendix A that the solution $h = h(y)$ of (36) subject to (13a) at $y = 0$ and (26) at $y = a$ has a single stationary point, a maximum $h = h_m$ at $y = 0$, and so the cross-sectional profile of the rivulet decreases monotonically from $h = h_m$ at $y = 0$ to $h = 0$ at $y = a$. The solution of (42) may therefore be written in the implicit form

$$y = \int_h^{h_m} \frac{1}{\left[f(\tilde{h})\right]^{1/2}}\,\mathrm{d}\tilde{h} \tag{44}$$

for $0 \leqslant y \leqslant a$, where the flux Q and semi-width a are given by

$$Q = \frac{2\sin\alpha}{3}\int_0^{h_m} \frac{\tilde{h}^3}{\left[f(\tilde{h})\right]^{1/2}}\,\mathrm{d}\tilde{h}, \tag{45}$$

$$a = \int_0^{h_m} \frac{1}{\left[f(\tilde{h})\right]^{1/2}}\,\mathrm{d}\tilde{h}. \tag{46}$$

One can also show that when $M > 0$ the function $h(y)$ always has a single point of inflection in $y > 0$, so that the cross-sectional profile steepens away from the contact line before flattening at the middle. On the other hand when $M < 0$ the profile may have up to two points of inflection in $y > 0$ when $\frac{1}{2}\pi < \alpha \leqslant \pi$, but has none when $0 \leqslant \alpha \leqslant \frac{1}{2}\pi$. In the isothermal case $M = 0$ the profile may have at most one point of inflection in $y > 0$ when $\frac{1}{2}\pi < \alpha \leqslant \pi$, but has none when $0 \leqslant \alpha \leqslant \frac{1}{2}\pi$.

https://doi.org/10.1017/S0022112001004797 Published online by Cambridge University Press

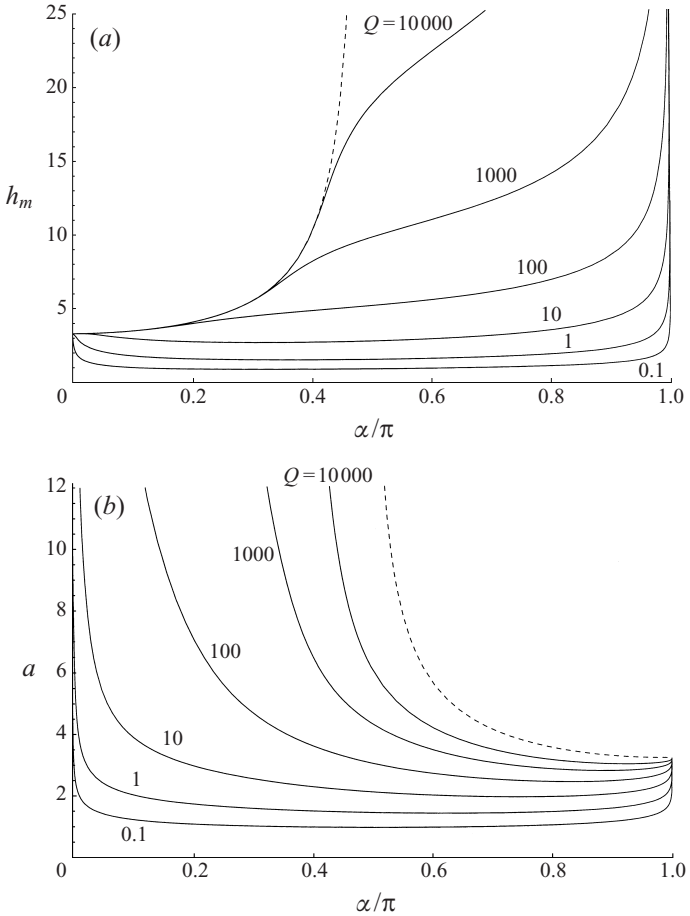


FIGURE 2. Numerically calculated solutions for (*a*) h_m and (*b*) a, plotted as functions of α/π for a range of values of Q when $M = 1$. The dashed curves show the leading-order solutions given in (66) and (67) for h_m and (69) for a in the limit $Q \to \infty$.

With Q prescribed, equation (45) is an algebraic equation determining h_m, and then equation (46) determines a explicitly, and (44) determines the profile $h(y)$ implicitly. This procedure was implemented numerically using the computer algebra package *Mathematica*, and analytically in appropriate asymptotic limits. In the remainder of this paper we shall describe in detail the properties of this implicit solution; in practice the parameter B is often small, and so for simplicity we shall largely restrict our attention to the adiabatic case $B = 0$ (see, for example, Tan *et al.* 1990 and Smith 1995).

It is convenient in the subsequent analytical calculations to write $\tilde{h} = th_m$ in (43)–(46) to obtain

$$y = h_m \int_{h/h_m}^{1} \frac{1}{[F(t)]^{1/2}}\,\mathrm{d}t, \tag{47}$$

$$Q = \frac{2h_m^4 \sin\alpha}{3} \int_0^1 \frac{t^3}{[F(t)]^{1/2}}\,\mathrm{d}t, \tag{48}$$

$$a = h_m \int_0^1 \frac{1}{[F(t)]^{1/2}}\,\mathrm{d}t, \tag{49}$$

https://doi.org/10.1017/S0022112001004797 Published online by Cambridge University Press

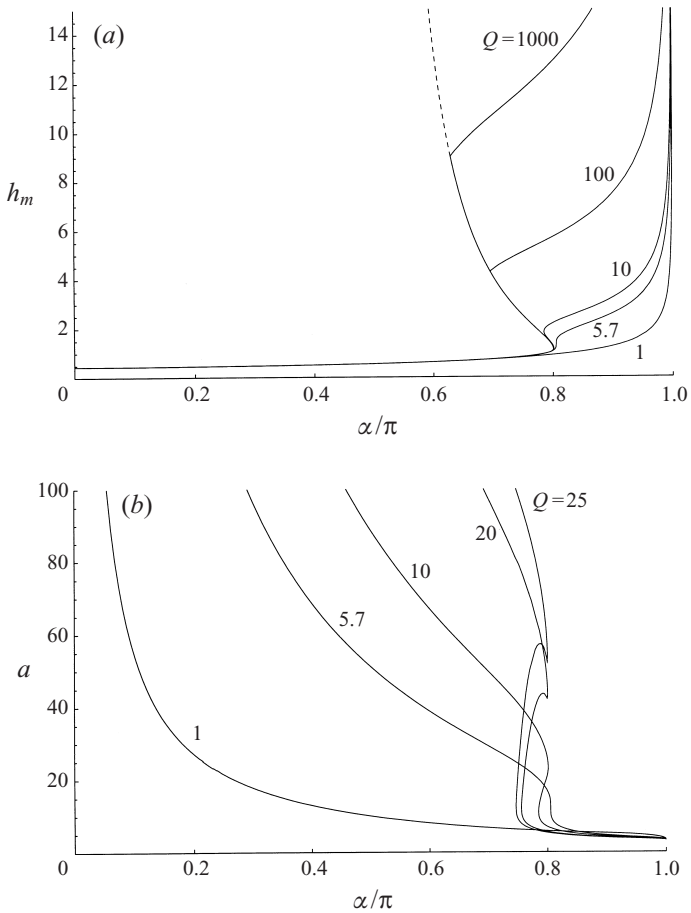


FIGURE 3. As for figure 2 except that $M = -0.6$. The dashed curve shows the leading-order solution on the middle branch in the limit $Q \to \infty$.

where we define $F(t)$ by $F(t) = f(\tilde{h})$, that is,

$$F(t) = (1-t)(1 - th_m^2 \cos\alpha) - 3Mh_m t \log\left(\frac{t(1+Bh_m)}{1+Bh_m t}\right). \tag{50}$$

Moreover, with (48) equation (49) may be written

$$a = \frac{3Q}{2h_m^3 \sin\alpha} + h_m \int_0^1 \frac{1-t^3}{[F(t)]^{1/2}}\,\mathrm{d}t. \tag{51}$$

In general the integrands in (47)–(49) are finite except when $t \to 1$, and from (50) we have

$$F(t) = C_1(1-t) + C_2(1-t)^2 + O(1-t)^3 \tag{52}$$

as $t \to 1$, where

$$C_1 = 1 - h_m^2 \cos\alpha + \frac{3Mh_m}{1+Bh_m}, \quad C_2 = h_m^2 \cos\alpha - \frac{3Mh_m}{2(1+Bh_m)^2}. \tag{53}$$

Since F must be positive as $t \to 1^-$ ($\tilde{h} \to h_m^-$) we have $C_1 \geqslant 0$, and we note that the singularities in (47)–(49) as $t \to 1$ are integrable if $C_1 > 0$.

https://doi.org/10.1017/S0022112001004797 Published online by Cambridge University Press

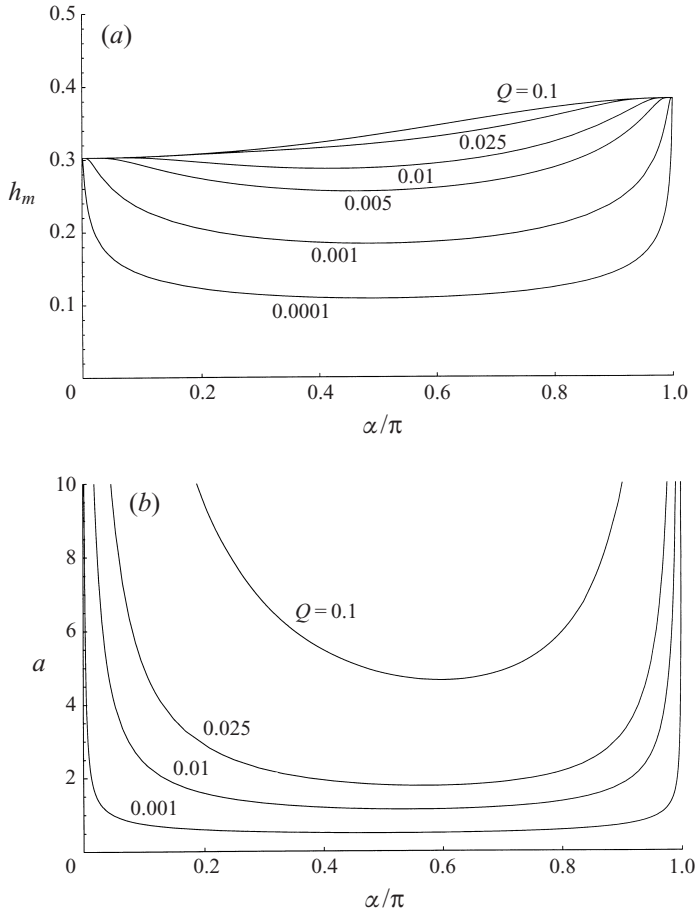


FIGURE 4. As for figure 2 except that $M = -1$. Note that in this case plots of h_m for $Q > 0.1$ are indistinguishable (at this scale) from that for $Q = 0.1$.

Examples of the variation of h_m and a with α, obtained from (48)–(50), are shown in figures 2, 3 and 4 for the cases $M = 1$, $M = -0.6$ and $M = -1$ respectively, for a range of values of Q, and in figures 5 and 6 for the case $Q = 1$ for a range of positive and negative values of M respectively.

It is found that for $M \geqslant 0$ and $M \leqslant -\frac{2}{3}$ there exists a solution in which h_m and a are single-valued functions of α for any Q, but that for $-\frac{2}{3} < M < 0$ there exists a critical flux Q_c such that h_m and a are single-valued for $Q \leqslant Q_c$ but are triple-valued over some interval $\alpha_1 \leqslant \alpha \leqslant \alpha_2$ for $Q > Q_c$; here $\alpha_1 > \frac{1}{2}\pi$ and $\alpha_0 < \alpha_2 < \pi$, where $\alpha_0 = \cos^{-1}(-9M^2/4)$ (so that $\frac{1}{2}\pi < \alpha_0 < \pi$, $\alpha_0 \to \frac{1}{2}\pi$ as $M \to 0^-$ and $\alpha_0 \to \pi$ as $M \to -\frac{2}{3}^+$). The form of h_m as a function of α in the case $-\frac{2}{3} < M < 0$ is sketched in figure 7, showing the 'middle' branch in $\alpha_1 \leqslant \alpha \leqslant \alpha_2$ connecting the 'lower' branch in $0 \leqslant \alpha \leqslant \alpha_2$ and the 'upper' branch in $\alpha_1 \leqslant \alpha \leqslant \pi$; examples are shown in figure 3 (in which $Q_c \simeq 5.7$).† The critical flux Q_c is determined by the condition that there is just one value of α in $\frac{1}{2}\pi < \alpha < \pi$ where $\mathrm{d}h_m/\mathrm{d}\alpha \to \infty$ (and $\mathrm{d}a/\mathrm{d}\alpha \to \infty$). Figure 8

† In figure 3 (a case satisfying $-\frac{2}{3} < M < 0$) some of the plots of both h_m and a would appear to have discontinuities in slope (corners) at certain points; in fact, on a finer scale it is seen that all the curves shown are smooth, though with high curvature at the apparent corners.

https://doi.org/10.1017/S0022112001004797 Published online by Cambridge University Press

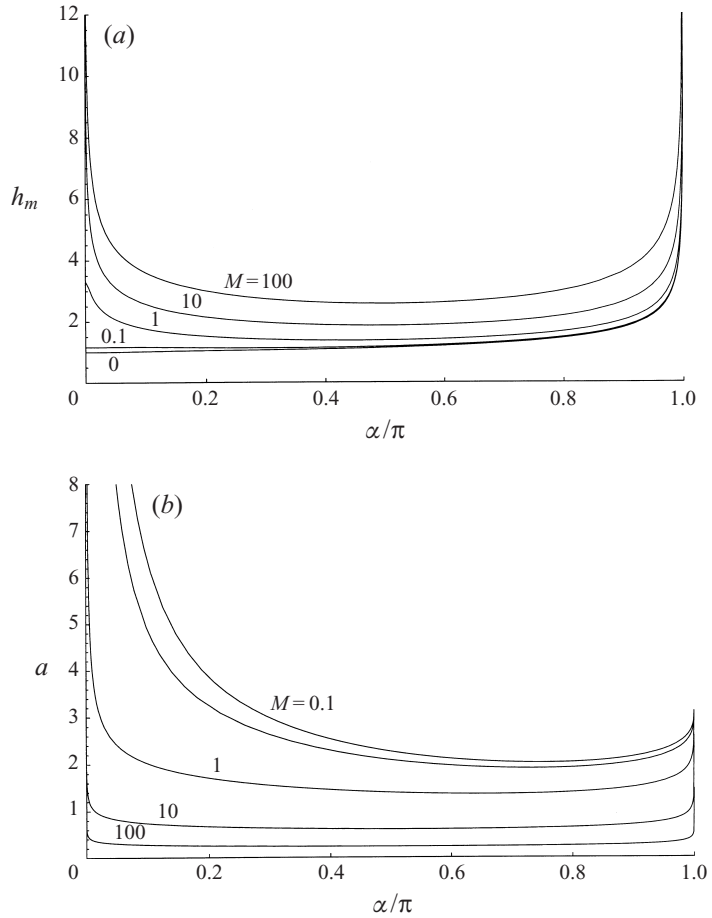


FIGURE 5. Numerically calculated solutions for (*a*) h_m and (*b*) a, plotted as functions of α/π for a range of positive values of M when $Q = 1$.

shows the variation of Q_c with $\bar{M}$ $(= -M)$ in the relevant interval $0 < \bar{M} < \frac{2}{3}$. We find that $Q_c \to \infty$ as $\bar{M} \to 0^+$ and $Q_c \to 0$ as $\bar{M} \to \frac{2}{3}^-$. In, for example, flow round a large horizontal cylinder, the maximum height of the rivulet corresponding to the solution in figure 7 would presumably 'jump' discontinuously between the lower and upper branches when α passes through α_1 or α_2, and so the solutions on the middle branch where $\mathrm{d}h_m/\mathrm{d}\alpha < 0$ would not be attained in practice; thus only discontinuous solutions occur when $Q > Q_c$ for $-\frac{2}{3} < M < 0$. On the other hand in flow down a plane inclined at an angle α satisfying $\alpha_1 < \alpha < \alpha_2$ there are three possible solutions. A stability analysis of the rivulet solutions obtained here is beyond the scope of the present paper, but a preliminary (quasi-static) stability analysis indicates that solutions on at least part of the middle branch are unstable; one might therefore conjecture that the middle-branch solutions are unstable, and so would never be observed in practice.

Figure 9 shows examples of the cross-sectional profile of the rivulet, given by (47), for a range of values of α in the cases $M = 1$, $M = -0.5$ and $M = -0.8$, with $Q = 1$ in each case. For $M = 1$ the profiles shown are qualitatively similar to those given by Duffy & Moffatt (1995) in the isothermal case $M = 0$. For $M = -0.5$ the profiles are

https://doi.org/10.1017/S0022112001004797 Published online by Cambridge University Press

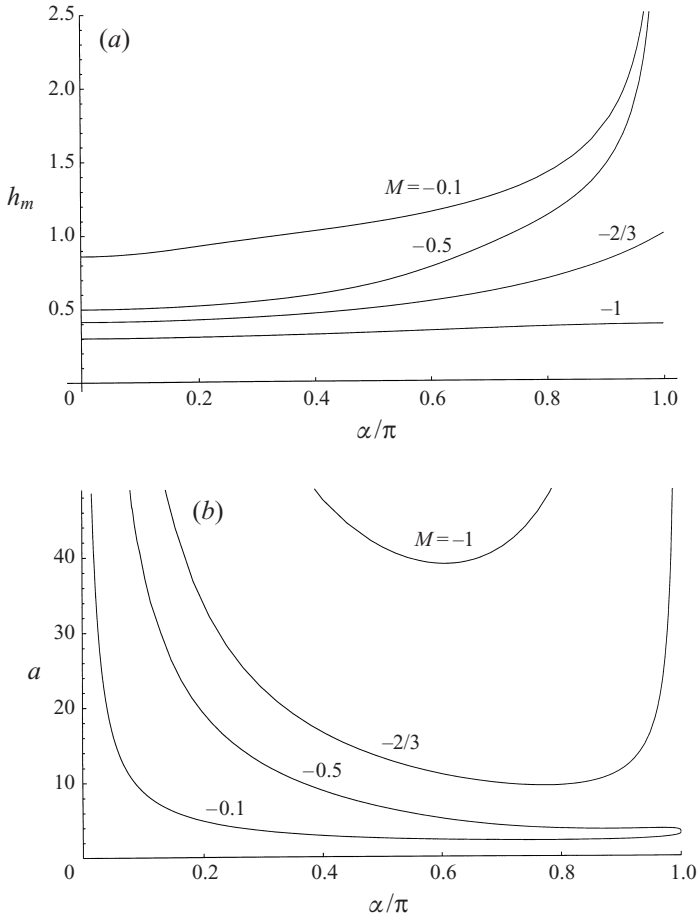


FIGURE 6. Numerically calculated solutions for (*a*) h_m and (*b*) a, plotted as functions of α/π for a range of negative values of M when $Q = 1$.

rather flat when $\alpha < \frac{1}{2}\pi$, except in a boundary layer near the contact line $y = a$, but are much narrower and more peaked when $\alpha > \frac{1}{2}\pi$. For $M = -0.8$ the profiles are very flat for all α, except in a boundary layer near $y = a$.

All of the general features of the solutions shown in the figures are captured well by appropriate asymptotic solutions, described below.

3.1. *The limit* $\alpha \to 0$

For the integral in (48) to be real valued in the limit $\alpha \to 0$ the maximum height of the rivulet h_m must approach a finite value, h_{m0} say. However, if $C_1 \neq 0$ when $\alpha = 0$ in (52) then the integral in (48) would be $O(1)$ as $\alpha \to 0$, and so (48) could not be satisfied. The only alternative is that $C_1 = 0$ when $\alpha = 0$, so that h_{m0} is given by

$$h_{m0} = \tfrac{1}{2}\left[3M + (9M^2 + 4)^{1/2}\right]; \tag{54}$$

this means that $C_2 = \frac{1}{2}(9M^2 + 4)^{1/2} h_{m0} > 0$ and that the integral in (48) is divergent. The expansion of the integrand in (48) for $t \to 1$ is non-uniform when $1 - t = O(\alpha^2)$;

https://doi.org/10.1017/S0022112001004797 Published online by Cambridge University Press

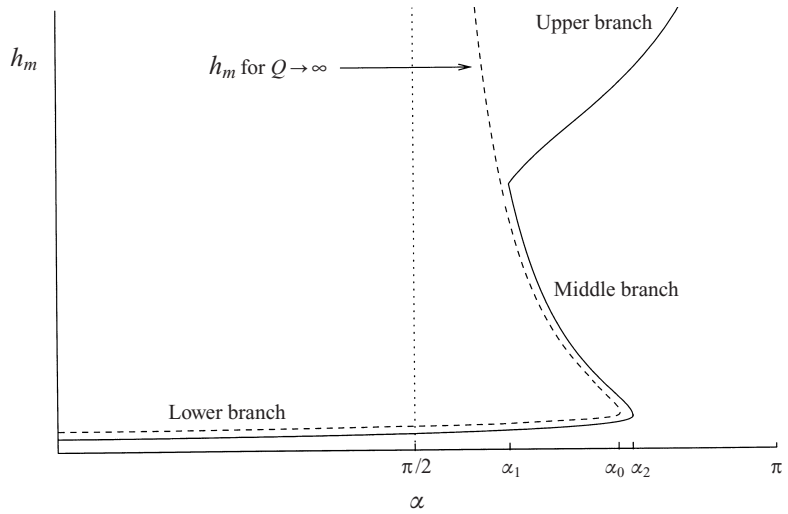


FIGURE 7. Sketch of the form of h_m as a function of α when $-\frac{2}{3} < M < 0$ and $Q > Q_c$. The angles α_1 and α_2 are where $\mathrm{d}h_m/\mathrm{d}\alpha \to \infty$, and $\alpha_0 = \cos^{-1}(-9M^2/4)$. The dashed curve represents the leading-order solution for h_m in the limit $Q \to \infty$ in this case.

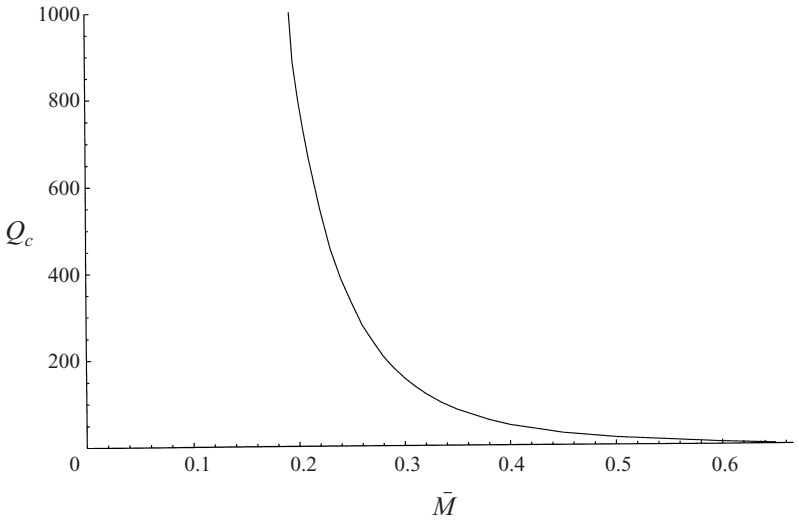


FIGURE 8. The critical flux Q_c plotted as a function of $\bar{M} = -M$ in the relevant interval $0 < \bar{M} < \frac{2}{3}$.

to determine subsequent terms in the expansion of h_m we therefore decompose the integral as the sum of integrals over the intervals $[0, 1-\delta_1]$ and $[1-\delta_1, 1]$, where $0 < \alpha^2 \ll \delta_1 \ll 1$, and obtain asymptotic approximations to these integrals separately (cf. Hinch 1991, p. 39). We thus find that

$$h_m = h_{m0} + \frac{h_{m0}^2 \alpha^2}{2(9M^2+4)^{1/2}} + O(\alpha^4) \tag{55}$$

as $\alpha \to 0$. Also the integral in (51) is $O(1)$ as $\alpha \to 0$, and we have

$$a = \frac{3Q}{2h_{m0}^3 \alpha} + h_{m0} \int_0^1 \frac{1-t^3}{[(1-t)(1-h_{m0}^2 t) - 3Mh_{m0} t \log t]^{1/2}} \, \mathrm{d}t + O(\alpha) \tag{56}$$

https://doi.org/10.1017/S0022112001004797 Published online by Cambridge University Press

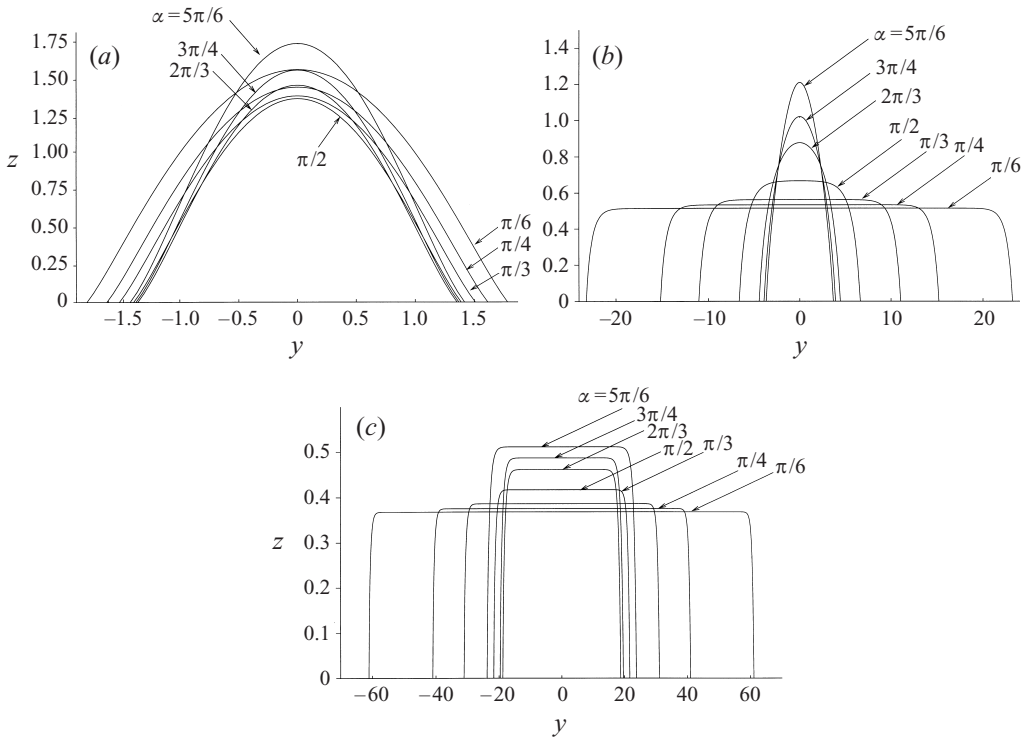


FIGURE 9. Transverse free-surface profiles for a range of values of α in the cases (a) $M = 1$, (b) $M = -0.5$ and (c) $M = -0.8$, when $Q = 1$.

as $\alpha \to 0$, showing that whereas h_m approaches the finite value h_{m0} in this limit, a is unbounded. These results collapse to those of Duffy & Moffatt (1995) in the case $M = 0$. Moreover (47) shows that the free-surface profile is flat, with $h(y) \sim h_{m0}$, except in a boundary layer near $y = a$.

3.2. *The limit* $\alpha \to \pi$

The behaviour of the solution in the limit $\alpha \to \pi$ is different in the two cases $M > -\frac{2}{3}$ and $M \leqslant -\frac{2}{3}$.

If $M > -\frac{2}{3}$ then in the limit $\alpha \to \pi$ there is no real positive value of h_m such that $C_1 = 0$, and so the integral in (48) is finite; this means that (48) can be satisfied only if $h_m \to \infty$ as $\alpha \to \pi$, which in turn means that the expansions of the integrands in (48) and (49) for $t \to 0$ are non-uniform when $t = O(h_m^{-2})$. Therefore, analogously to the case $\alpha \to 0$ described in § 3.1, we treat each integral by decomposing it as a sum of integrals over $[0, \delta_2]$ and $[\delta_2, 1]$, where $0 < h_m^{-2} \ll \delta_2 \ll 1$. We thus find that

$$h_m = \left(\frac{24Q}{5\pi(\pi - \alpha)}\right)^{1/3} + \left(\frac{47}{10} - 6\log 2\right) M + o(1), \tag{57}$$

$$a = \pi - (2 + 3\pi M)\left(\frac{5\pi(\pi - \alpha)}{24Q}\right)^{1/3} + o(\pi - \alpha)^{1/3} \tag{58}$$

https://doi.org/10.1017/S0022112001004797 Published online by Cambridge University Press

as $\alpha \to \pi$ when $M > -\frac{2}{3}$, showing that whereas h_m is unbounded in this limit,† a approaches the finite value π. Again these results reduce to those of Duffy & Moffatt (1995) in the case $M = 0$. Moreover from (47) the free-surface profile is given by

$$h(y) \sim h_m \cos^2 \tfrac{1}{2} y \tag{59}$$

(which satisfies $h(a) = 0$ and $h_y(a) = o(\pi - \alpha)^{-1/3}$, consistent with (26)). Also we note that in figure 6(*b*) the difference in sign of the slope of a at $\alpha = \pi$ between the cases $M = -0.1$ and $M = -0.5$ is in agreement with (58), which predicts a change of sign between $M < -2/3\pi$ ($\simeq -0.2122$) and $M > -2/3\pi$.

If $M \leqslant -\frac{2}{3}$ then in the limit $\alpha \to \pi$ we find that although there is still a solution of the type (57)–(59) with h_m unbounded there is also a solution in which h_m remains finite; in that case (48) can be satisfied only if $C_1 = 0$, which determines h_m at leading order, and then a at leading order is obtained straightforwardly from (51). We thus find, analogously to (55) and (56), that

$$h_m = h_{m\pi} - \frac{h_{m\pi}^2(\pi - \alpha)^2}{2(9\bar{M}^2 - 4)^{1/2}} + O(\pi - \alpha)^4, \tag{60}$$

$$a = \frac{3Q}{2h_{m\pi}^3(\pi - \alpha)} + h_{m\pi} \int_0^1 \frac{1 - t^3}{[(1 - t)(1 + h_{m\pi}^2 t) + 3\bar{M} h_{m\pi} t \log t]^{1/2}} \, \mathrm{d}t + O(\pi - \alpha) \tag{61}$$

as $\alpha \to \pi$ when $\bar{M} = -M \geqslant \frac{2}{3}$, where

$$h_{m\pi} = \tfrac{1}{2} \left[3\bar{M} - (9\bar{M}^2 - 4)^{1/2}\right]. \tag{62}$$

Equations (60)–(61) show that whereas h_m approaches the finite value $h_{m\pi}$ in this limit, a is unbounded. Moreover (47) shows that the free-surface profile is flat, with $h(y) \sim h_{m\pi}$, except in a boundary layer near $y = a$.

3.3. *The limit* $Q \to 0$

In the limit of small flux $Q \to 0$ equation (48) can be satisfied only if the outer solution for h_m (valid away from $\alpha = 0$ and $\alpha = \pi$) satisfies $h_m \to 0$. It is then found that the integrals in (48) and (49) are dominated by 'global contributions' (Hinch 1991, p. 37) for small h_m; we thus find that

$$h_m = \frac{1}{2} \left(\frac{105Q}{4 \sin \alpha}\right)^{1/4} + \frac{M}{32}(840 \log 2 - 533) \left(\frac{3Q}{35 \sin \alpha}\right)^{1/2} + o(Q^{1/2}), \tag{63}$$

$$a = \left(\frac{105Q}{4 \sin \alpha}\right)^{1/4} - \frac{113M}{16} \left(\frac{3Q}{35 \sin \alpha}\right)^{1/2} + o(Q^{1/2}) \tag{64}$$

as $Q \to 0$, so that both h_m and a are $O(Q^{1/4})$. Moreover from (47) the free-surface profile is given by

$$h(y) \sim h_m \left(1 - \frac{y^2}{a^2}\right). \tag{65}$$

Comparison with (55)–(61) shows that the solution (63)–(65) fails near $\alpha = 0$ and $\alpha = \pi$ where there are boundary layers of width $O(Q)$, within which both h_m and a are $O(1)$ at leading order in Q; however, the (implicit) expressions for h_m and a at

† Of course, the singular nature of h_m as $\alpha \to \pi$ means that the lubrication approximation breaks down in this limit; in the case of flow round a cylinder, an alternative approach would therefore be needed to describe the flow in the neighbourhood of the bottom of the cylinder $\alpha = \pi$.

https://doi.org/10.1017/S0022112001004797 Published online by Cambridge University Press

leading order in the boundary layers are only slightly simpler than the general results (48) and (49), so we omit the details for the sake of brevity.

These results are valid, in particular, in the case $M = 0$ considered by Duffy & Moffatt (1995), who did not investigate the limit $Q \to 0$.

3.4. *The limit $Q \to \infty$*

The behaviour of the solution in the limit of large flux $Q \to \infty$ is different in the three cases $M \geqslant 0$, $-\frac{2}{3} < M < 0$ and $M \leqslant -\frac{2}{3}$.

In the case $M \geqslant 0$ the outer solution (valid away from $\alpha = \frac{1}{2}\pi$) has different forms in the intervals $0 \leqslant \alpha < \frac{1}{2}\pi$ and $\frac{1}{2}\pi < \alpha \leqslant \pi$.

When $0 \leqslant \alpha < \frac{1}{2}\pi$ the maximum height h_m must be finite for the integral in (48) to be real, but then (48) can be satisfied only if $C_1 = 0$. This determines h_m at leading order, and a at leading order is then obtained straightforwardly from (51); we thus find that

$$h_m \sim H, \quad a \sim \frac{3Q}{2H^3 \sin\alpha} \tag{66}$$

as $Q \to \infty$ when $0 \leqslant \alpha < \frac{1}{2}\pi$, where

$$H = \frac{3M + (9M^2 + 4\cos\alpha)^{1/2}}{2\cos\alpha}, \tag{67}$$

showing that whereas h_m approaches the finite value H in this limit, a is unbounded. As $\alpha \to \frac{1}{2}\pi^-$ we have $H \sim 3M/(\frac{1}{2}\pi - \alpha)$ if $M > 0$ and $H \sim (\frac{1}{2}\pi - \alpha)^{-1/2}$ if $M = 0$. Moreover (47) shows that the free-surface profile is flat, with $h(y) \sim H$, except in a boundary layer near $y = a$. The leading-order solution for h_m given by (66) and (67) is shown as the dashed curve in figure 2(*a*). We note that (66) and (67) agree with (54)–(56) at leading order in the limit $\alpha \to 0$.

When $\frac{1}{2}\pi < \alpha \leqslant \pi$ we have $C_1 > 0$ for all h_m, and so the integral in (48) is finite; this means that (48) can be satisfied only if $h_m \to \infty$ as $Q \to \infty$, which in turn means that the expansions of the integrands in (48) and (49) for $t \to 0$ are non-uniform when $t = O(h_m^{-2})$. We therefore evaluate each integral via the procedure described in § 3.2; we thus find that

$$h_m = \left(\frac{24QG}{5\pi\sin\alpha}\right)^{1/3} + \left(\frac{47}{10} - 6\log 2\right)\frac{M}{G^2} + o(1), \tag{68}$$

$$a = \frac{\pi}{G} - \left(\frac{2G + 3\pi M}{G^3}\right)\left(\frac{5\pi\sin\alpha}{24QG}\right)^{1/3} + o(Q^{-1/3}) \tag{69}$$

as $Q \to \infty$ when $\frac{1}{2}\pi < \alpha \leqslant \pi$ (where $G = |\cos\alpha|^{1/2}$), showing that whereas h_m is unbounded in this limit, a approaches the finite value π/G. Moreover from (47) the free-surface profile is given by

$$h(y) \sim h_m \cos^2 \tfrac{1}{2}Gy \tag{70}$$

(which satisfies $h(a) = 0$ and $h_y(a) = o(Q^{1/3})$, consistent with (26)). The leading-order solution for a in (69) is shown as the dashed curve in figure 2(*b*). Also we note that (68)–(70) agree with (57)–(59) in the limit $\alpha \to \pi$.

Clearly the solution (66)–(70) fails near $\alpha = \frac{1}{2}\pi$ where there is a boundary layer across which h_m and a change from their $O(1)$ and $O(Q)$ values in $0 \leqslant \alpha < \frac{1}{2}\pi$ to their $O(Q^{1/3})$ and $O(1)$ values in $\frac{1}{2}\pi < \alpha \leqslant \pi$. The nature of this layer depends on

https://doi.org/10.1017/S0022112001004797 Published online by Cambridge University Press

the size of M. When $M = O(1)$ the layer has thickness $O(Q^{-2/7})$, and within it h_m is $O(Q^{2/7})$ and a is $O(Q^{1/7})$. When $M = 0$, or more generally when $M = o(Q^{-1/4})$, the layer has thickness $O(Q^{-1/2})$, and within it both h_m and a are $O(Q^{1/4})$. Again we omit the details for the sake of brevity.

These results are valid, in particular, in the case $M = 0$ considered by Duffy & Moffatt (1995), who did not investigate the limit $Q \to \infty$.

In the case $M \leqslant -\frac{2}{3}$ we find that in the limit $Q \to \infty$ the leading-order solutions for h_m and a are given by (66) and (67) across the entire interval $0 < \alpha < \pi$ (see figure 4); in particular we have $H \to -\frac{1}{3}M$ as $\alpha \to \frac{1}{2}\pi$ when $M < 0$. Also we note that (66) and (67) agree with (60)–(62) at leading order in the limit $\alpha \to \pi$.

In the intermediate case $-\frac{2}{3} < M < 0$ the solutions h_m and a are triple-valued over the interval $\alpha_1 \leqslant \alpha \leqslant \alpha_2$ when $Q \to \infty$, with $\alpha_1 \to \frac{1}{2}\pi$ and $\alpha_2 \to \alpha_0 = \cos^{-1}(-9M^2/4)$. We find that the leading-order solutions for h_m and a are given by (66) and (67) on the lower branch ($0 \leqslant \alpha \leqslant \alpha_0$) and by (68) and (69) on the upper branch ($\frac{1}{2}\pi < \alpha < \pi$); see figures 3 and 7. On the middle branch ($\frac{1}{2}\pi < \alpha \leqslant \alpha_0$) the integral in (48) is dominated by a contribution from a double zero $t = t_0 \neq 1$ of $F(t)$, so that $F(t_0) = 0$ and $F'(t_0) = 0$, and therefore $F(t_0) - t_0F'(t_0) = 0$. The latter has relevant root $t_0 = H/h_m$ (where H is given by (67)), and so h_m at leading order in the limit $Q \to \infty$ on the middle branch is the relevant solution of the equation $F(H/h_m) = 0$; this is shown as the dashed curve in figure 3(*a*), lying in the interval $\frac{1}{2}\pi < \alpha \leqslant \alpha_0 \simeq 0.8005\pi$ for $M = -0.6$.

3.5. *The limit* $M \to 0$

The solution in the limit of weak heating or cooling $M \to 0$ is perhaps most easily obtained directly from the differential equation (37) and the boundary and flux conditions (rather than from the implicit solution (43)–(46)) by expanding h, h_m and a in powers of M in the form

$$h = h_0 + Mh_1 + O(M^2), \quad h_m = h_{m0} + Mh_{m1} + O(M^2), \quad a = a_0 + Ma_1 + O(M^2), \tag{71}$$

and solving the problem that emerges at each order in M. Details of this (rather lengthy) calculation are relegated to Appendix B, in which it is shown that the results of Duffy & Moffatt (1995) for the isothermal case are recovered at leading order, and in which the $O(M)$ terms in (71) are derived. Figure 10 shows the variation of h_{m1} and a_1 as functions of α for a range of values of Q, and in particular shows that $h_{m1} > 0$ and $a_1 < 0$. The behaviour of the first-order solution in the limits $\alpha \to 0$, $\alpha \to \pi$, $Q \to 0$ and $Q \to \infty$ is given by the appropriate expansions of the relevant results in §§ 3.1–3.4 and so need not be reiterated here.

3.6. *The limit* $M \to \infty$

In the limit of strong heating $M \to \infty$ equation (48) can be satisfied only if the outer solution for h_m (valid away from $\alpha = 0$ and $\alpha = \pi$) satisfies $h_m \to \infty$ and $h_m = o(M)$. Then the integrals in (48) and (49) are dominated by global contributions with integrands $t^{5/2}(-3Mh_m \log t)^{-1/2}$ and $(-3Mh_m t \log t)^{-1/2}$; we thus find that

$$h_m \sim \left(\frac{189Q^2M}{8\pi \sin^2\alpha}\right)^{1/7}, \quad a \sim \left(\frac{4\sqrt{7}\pi^3 Q}{9M^3 \sin\alpha}\right)^{1/7} \tag{72}$$

as $M \to \infty$, showing that $h_m \to \infty$ and $a \to 0$ in this limit, that is, the rivulet becomes deep and narrow (see figure 5). Moreover (47) shows that the free-surface profile is

https://doi.org/10.1017/S0022112001004797 Published online by Cambridge University Press

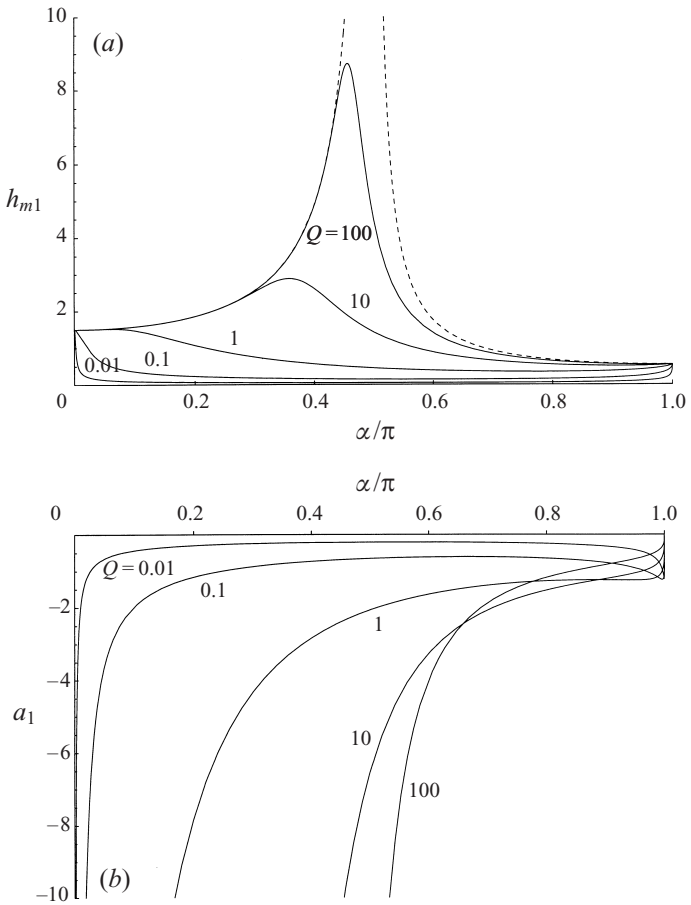


FIGURE 10. Solutions for (*a*) h_{m1} and (*b*) a_1, plotted as functions of α/π for a range of values of Q. The dashed curves in (*a*) show the $O(M)$ terms that arise in small-M expansions of the large-Q results (66) and (68) for $0 \leqslant \alpha < \frac{1}{2}\pi$ and $\frac{1}{2}\pi < \alpha \leqslant \pi$ respectively.

given by

$$h(y) \sim h_m \exp\left\{-2\left[\mathrm{erf}^{-1}\left(\frac{y}{a}\right)\right]^2\right\} \tag{73}$$

(where erf^{-1} denotes the inverse of the error function); this satisfies the boundary conditions (13*a*) and (26*a*) identically, and gives $h_y(a) = o(M^{1/7})$, consistent with (26*b*). The solution (73) is analogous to the solution given by Ehrhard & Davis (1991, Appendix) for the steady profile of a two-dimensional drop in the case when gravity is negligible and the contact angle is zero.

Comparison of (72) with (55)–(58) shows that this solution fails near $\alpha = 0$ and $\alpha = \pi$ where there are boundary layers of thickness $O(M^{-3})$, within which h_m is $O(M)$ and a is $O(1)$. Again we omit the details for the sake of brevity.

3.7. *The limit $M \to -\infty$*

In the limit of strong cooling $\bar{M} = -M \to \infty$ equation (48) can be satisfied only if $h_m = O(\bar{M}^{-1})$ and $C_1 = 0$ in (52), giving $h_m \sim (3\bar{M})^{-1}$; then (51) gives $a \sim 81Q\bar{M}^3/2\sin\alpha$. In fact, writing $h_m = H - \delta$, where H is given by (67) and $0 < \delta \ll H$,

https://doi.org/10.1017/S0022112001004797 Published online by Cambridge University Press

we find that the integral in (48) is dominated by a global contribution with integrand $t^3[3\bar{M}\delta(1-t)]^{-1/2}$, and that the expression for a in (51) is dominated by the first term; thus

$$h_m \sim H - \left(\frac{64\sin\alpha}{105Q}\right)^2 \frac{1}{(3\bar{M})^9}, \quad a \sim \frac{3Q}{2H^3\sin\alpha} \tag{74}$$

as $\bar{M} = -M \to \infty$. Since $H \sim (3\bar{M})^{-1}$, equation (74) shows that $h_m \to 0$ and $a \to \infty$ in this limit, that is, the rivulet becomes shallow and wide (see figure 6); also h_m coincides with H up to $O(\bar{M}^{-9})$. Moreover (47) shows that the free-surface profile is flat, with $h(y) \sim H$, except in a boundary layer near $y = a$.

3.8. *Comparison between numerical and asymptotic results*

Detailed comparisons show that in general the asymptotic solutions given above can provide a very accurate representation of the exact (numerical) solutions obtained directly from (47)–(50). For example, for $M = 1$ the small-Q asymptotic solution for h_m would be virtually indistinguishable from the exact solution in figure 2(*a*) for $Q = 0.1$, and for $M = -1$ the large-Q asymptotic solution for h_m would be indistinguishable from the exact solution in figure 4(*a*) even for Q as small as $Q = 0.1$. (It is for this reason that the solutions are plotted for only relatively small values of Q in figure 4: the solutions h_m for larger values of Q would be indistinguishable from that for $Q = 0.1$.) Similarly for $Q = 1$ the small-M and large-positive-M asymptotic solutions for h_m would be indistinguishable from the exact solutions in figure 5(*a*) for $M = 0.1$ and $M = 10$ respectively, and the small-M and large-negative-M asymptotic solutions for h_m would be indistinguishable from the exact solutions in figure 6(*a*) for $M = -0.1$ and $M = -1$ respectively.

4. The transverse flow

As we have already seen in § 2, the thermocapillary effect drives a transverse flow (absent in the isothermal case), so that overall the fluid particles spiral down the rivulet in helical vortices. Using (31) and (32) with p, h_{yyyy} and h_{yyy} substituted from (28) and (36) we may write the transverse velocity components v and w as

$$v = \frac{Mh_y z(3z-2h)}{4h(1+Bh)^2}, \tag{75}$$

$$w = \frac{Mz^2}{4h^2(1+Bh)^3}\left[h(1+Bh)(h-z)h_{yy} + h_y^2\big(z+Bh(3z-2h)\big)\right]. \tag{76}$$

We consider a projection of this flow onto the transverse (y,z)-plane, in which we may define a 'stream function' ψ by $v = -\psi_z$ and $w = \psi_y$, with $\psi = 0$ on $z = 0$, so that

$$\psi(y,z) = \frac{Mh_y z^2(h-z)}{4h(1+Bh)^2}. \tag{77}$$

Evidently $\psi = 0$ on $z = 0$, on $z = h$ and on the symmetry axis $y = 0$. If $M > 0$ then $\psi \leqslant 0$ in $0 \leqslant y \leqslant a$ (since $h_y \leqslant 0$ there), and conversely if $M < 0$ then $\psi \geqslant 0$ in $0 \leqslant y \leqslant a$. Furthermore if $M = 0$ then $\psi = 0$ and $v = w = 0$, confirming the absence of a transverse flow in the isothermal problem.

At any 'stagnation points' of the transverse flow we have $v = w = 0$, which lead either to $y = 0$, $z = h_m$ (a stagnation saddle point at the 'apex' of the rivulet) or to

$$z = \tfrac{2}{3}h, \quad h(1+Bh)h_{yy} + 2h_y^2 = 0. \tag{78}$$

https://doi.org/10.1017/S0022112001004797 Published online by Cambridge University Press

From (42) we may substitute for h_y^2 and h_{yy} in terms of h into (78) to obtain an algebraic equation for h, namely $h(1+Bh)f'(h)+4f(h)=0$, that is,

$$2Bh_mh^3\cos\alpha+[6h_m\cos\alpha-B(1+h_m^2\cos\alpha)]h^2-5(1+h_m^2\cos\alpha)h$$
$$-3Mh_mh+4h_m-3Mh_mh(5+Bh)\log\left(\frac{h(1+Bh_m)}{h_m(1+Bh)}\right)=0. \qquad (79)$$

If this equation has a solution $h=h_s$ in the interval $0<h_s<h_m$, then there is a stagnation point in $0<y<a$, at (y_s,z_s) say, where

$$z_s=\tfrac{2}{3}h_s, \quad y_s=\int_{h_s}^{h_m}\frac{\mathrm{d}\tilde{h}}{[f(\tilde{h})]^{1/2}} \quad (0<y_s<a). \qquad (80)$$

When $B=0$ one can show that, except in the case when $-\frac{2}{3}<M<0$ and $-225M^2/96<\cos\alpha<0$, equation (79) has a unique solution $h=h_s$ in $0<h_s<h_m$. Thus in the transverse (y,z)-plane the streamlines in $y>0$ are closed curves, and the flow comprises a single closed eddy, with all particles circulating round the stagnation point (y_s,z_s). In flow down an inclined plane the time τ taken by particles to complete one circuit of the eddy varies from $\tau=0$ (for a particle at the stagnation point (y_s,z_s)) to $\tau\to\infty$ (for a particle on the bounding streamline $\psi=0$). In flow down a slowly varying substrate a somewhat similar statement concerning particle travel times is expected to be valid, but, of course, the eddy in which any particular particle moves will, in general, be different from one station α to another. When $-\frac{2}{3}<M<0$ and $-225M^2/96<\cos\alpha<0$ there are cases when (79) has three solutions $h=h_s$ in $0<h_s<h_m$, so there are three stagnation points in $0<y<a$, namely a stagnation saddle point between two 'elliptic' stagnation points, all lying on the curve $z=\frac{2}{3}h$. Thus in the transverse (y,z)-plane the streamlines in $y>0$ are again closed curves, but the flow comprises two 'internal' eddies (circulating fluid bounded by the 'saddle connections') which in turn are surrounded by circulating fluid. These cases can occur both when $Q\leqslant Q_c$ (relevant to the flow of a continuous rivulet round a large cylinder) and when $Q>Q_c$ with h_m lying on the middle or upper branches.

Examples of the transverse streamline patterns are shown for various cases in figures 11–13. For $M>0$ the free-surface temperature is greater near the contact line $y=a$ than it is near the symmetry axis $y=0$, so the surface tension is stronger near $y=0$ than it is near $y=a$; this drives a motion in which particles near the free surface $z=h(y)$ move towards $y=0$, and so particles near the substrate $z=0$ move towards $y=a$, that is, the circulation in $y>0$ is anticlockwise in figures with $M>0$. For increasing M (that is, for stronger heating) a stronger transverse flow is generated, and the rivulet becomes narrower and deeper, as shown in figure 5. For $M<0$ the situation is reversed, that is, the transverse circulation in $y>0$ is clockwise, and the rivulet becomes shallower and wider with increasing $|M|$, as shown in figure 6.

From (77) any streamline $\psi=$ constant may be expressed explicitly (in terms of the known function $h(y)$) by

$$z=\tfrac{1}{3}h\left[1+2\cos\left\{\tfrac{1}{3}\pi\pm\tfrac{1}{3}\cos^{-1}\left(-1-\frac{54(1+Bh)^2\psi}{Mh^2[f(h)]^{1/2}}\right)\right\}\right], \qquad (81)$$

the $\pm$ sign here representing the 'lower' and 'upper' arcs of the closed streamline, which meet 'vertically' on the curve $z=\frac{2}{3}h$, at points where

$$-\frac{Mh^2[f(h)]^{1/2}}{27(1+Bh)^2}=\psi. \qquad (82)$$

https://doi.org/10.1017/S0022112001004797 Published online by Cambridge University Press

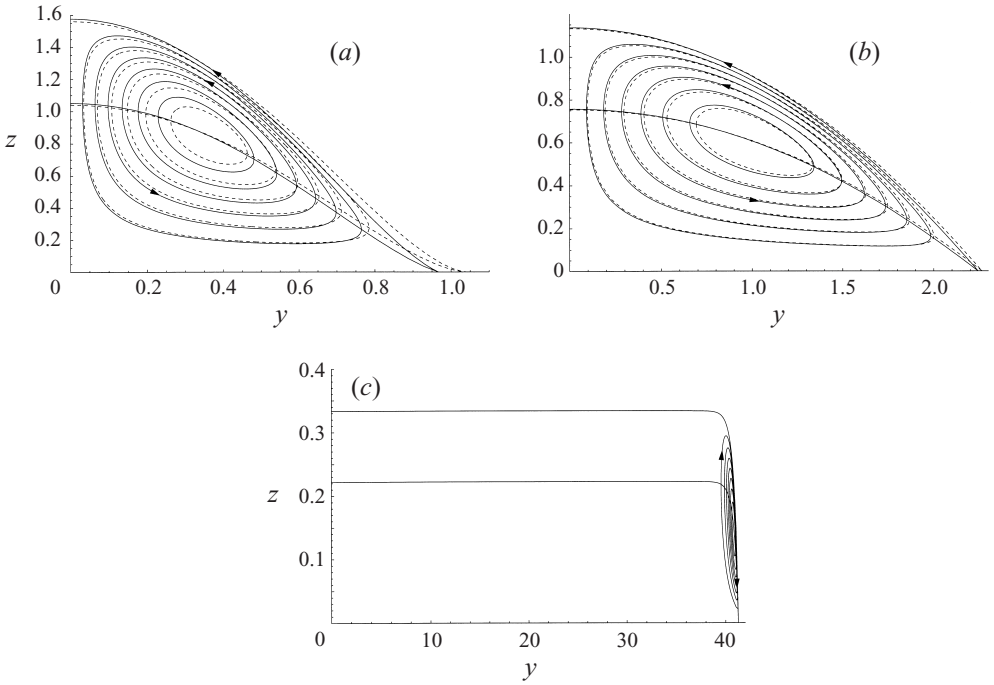


FIGURE 11. Streamlines of the transverse flow at $\alpha = \frac{1}{2}\pi$ in the cases (*a*) $Q = 1$, $M = 0.01$, (*b*) $Q = 1$, $M = 3$, and (*c*) $Q = 0.01$, $M = -1$. The curves $z = \frac{2}{3}h$ (which the streamlines cross 'vertically') are also shown. In cases (*a*) and (*b*) the dashed curves show the leading-order composite streamlines in the limits $M \to 0$ and $M \to \infty$ respectively.

In particular at any stagnation point (y_s, z_s) we have $\psi = \psi_s$, where

$$\psi_s = -\frac{Mh_s^2[f(h_s)]^{1/2}}{27(1+Bh_s)^2}. \tag{83}$$

The quantity ψ_s (or, in cases where there are three stagnation points in $0 < y < a$, the largest of the three values ψ_s) may be regarded as a measure of flux circulating in the transverse plane; the complete family of streamlines in $0 \leqslant y \leqslant a$ is obtained by taking $\psi_s \leqslant \psi \leqslant 0$ (for $M > 0$) or $0 \leqslant \psi \leqslant \psi_s$ (for $M < 0$) in (81).

In the limit $M \to 0$ the stream function ψ takes the form

$$\psi = \psi_0 + M\psi_1 + O(M^2), \tag{84}$$

with $\psi_0 = 0$ and

$$\psi_1 = \frac{h_{0y}z^2(h_0 - z)}{4h_0(1+Bh_0)^2}, \tag{85}$$

where h_0 is given by (B 3) in Appendix B. From (78) the position of the stagnation point in the case $B = 0$ is given at leading order by

$$y_s = \begin{cases} \dfrac{1}{G}\cosh^{-1}\left[\frac{1}{6}\left\{\cosh Ga_0 + (24 + \cosh^2 Ga_0)^{1/2}\right\}\right] & \text{if} \quad 0 \leqslant \alpha < \frac{1}{2}\pi, \\ \dfrac{a_0}{\sqrt{5}} & \text{if} \quad \alpha = \frac{1}{2}\pi, \\ \dfrac{1}{G}\cos^{-1}\left[\frac{1}{6}\left\{\cos Ga_0 + (24 + \cos^2 Ga_0)^{1/2}\right\}\right] & \text{if} \quad \frac{1}{2}\pi < \alpha \leqslant \pi, \end{cases} \tag{86}$$

https://doi.org/10.1017/S0022112001004797 Published online by Cambridge University Press

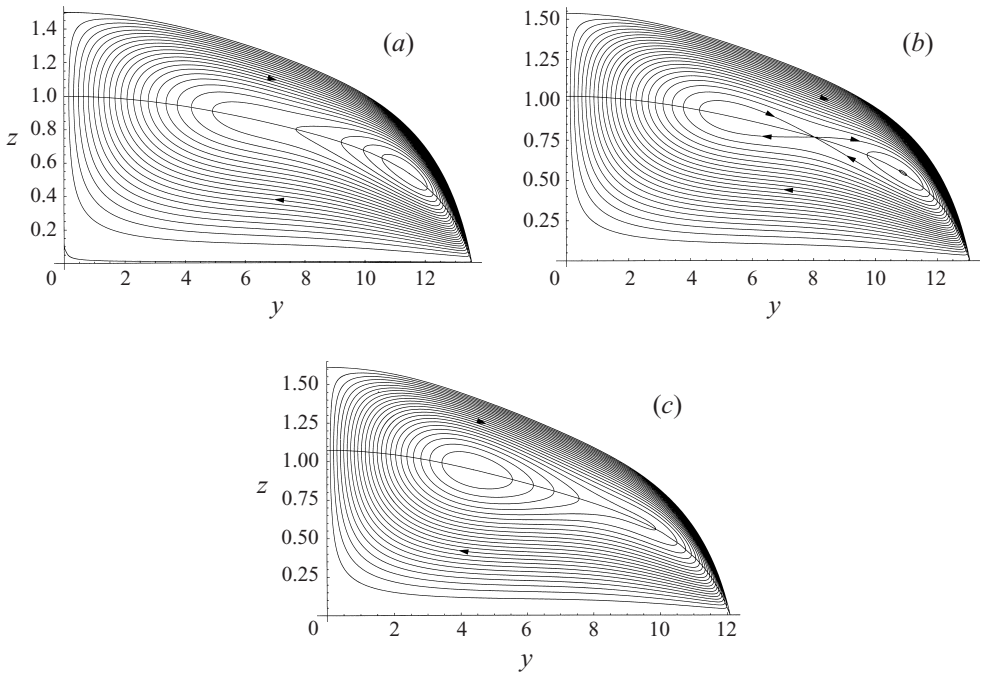


FIGURE 12. Streamlines of the transverse flow in the case $M = -0.5$ and $Q = 14$ ($< Q_c \simeq 17.0$), at (a) $\alpha = 2.181$, (b) $\alpha = 2.182$, and (c) $\alpha = 2.1842$. The curves $z = \frac{2}{3}h$ (which the streamlines cross 'vertically') are also shown.

$$z_s = \begin{cases} \dfrac{5\cosh Ga_0 - (24 + \cosh^2 Ga_0)^{1/2}}{9G\sinh Ga_0} & \text{if} \quad 0 \leqslant \alpha < \frac{1}{2}\pi, \\ \dfrac{4a_0}{15} & \text{if} \quad \alpha = \frac{1}{2}\pi, \\ \dfrac{-5\cos Ga_0 + (24 + \cos^2 Ga_0)^{1/2}}{9G\sin Ga_0} & \text{if} \quad \frac{1}{2}\pi < \alpha \leqslant \pi, \end{cases} \tag{87}$$

where again $G = |\cos\alpha|^{1/2}$. In particular $z_s/h_m \to \frac{4}{9}$ and $y_s \sim a_0 - \log 3$ (with $h_m \to 1$ and $a_0 \to \infty$) as $\alpha \to 0$; also $z_s/h_m \to \frac{5}{9}$ and $y_s \to \cos^{-1}\frac{2}{3} \simeq 0.8411 \simeq 0.2677a_0$ (with $h_m \to \infty$ and $a_0 \to \pi$) as $\alpha \to \pi$.

In the limit $M \to \infty$ the stream function ψ and the position (y_s, z_s) of the stagnation point are given at leading order by substituting the leading-order expression (73) for h into (77) and (78) respectively; when $B = 0$ the latter leads to

$$y_s \sim \operatorname{erf}\left(\frac{1}{\sqrt{10}}\right) a^{(0)} \simeq 0.3453a^{(0)}, \quad z_s \sim \tfrac{2}{3}\mathrm{e}^{-1/5}h_m^{(0)} \simeq 0.5458h_m^{(0)}, \tag{88}$$

where $h_m^{(0)}$ and $a^{(0)}$ are the leading-order outer solutions for h_m and a given in (72).

In the limit $M \to -\infty$ we find at leading order that $\psi = 0$ except in the boundary layer near $y = a$; thus fluid particles in the 'bulk' of the rivulet essentially undergo a local rectilinear flow, and the transverse flow is confined to the boundary layer.

Figure 11 shows examples of the streamline patterns of the transverse flow at $\alpha = \frac{1}{2}\pi$ (in which case there is only ever one eddy in $0 < y < a$). Figures 11(a) and 11(b) are for the cases $M = 0.01$ and $M = 3$, with $Q = 1$ in both. For comparison the leading-order composite streamlines in the limits $M \to 0$ and $M \to \infty$, obtained from

https://doi.org/10.1017/S0022112001004797 Published online by Cambridge University Press

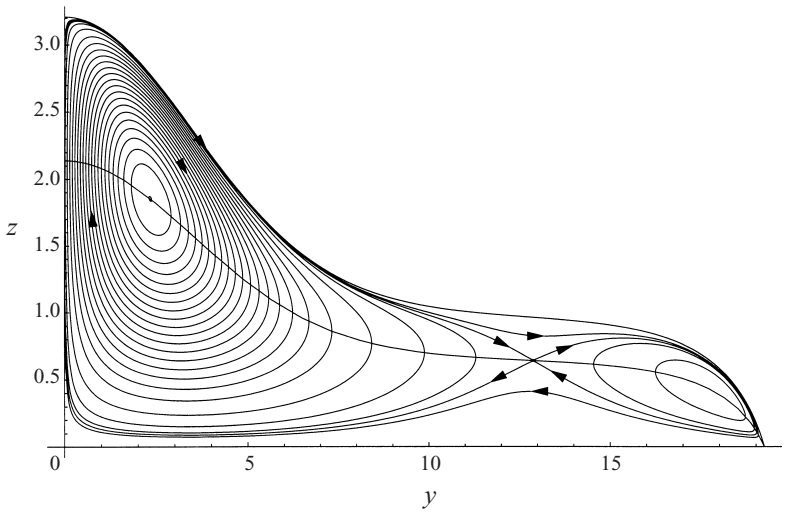


FIGURE 13. Streamlines of the transverse flow in the case $\alpha = 2.072$, $M = -0.5$ and $Q = 70$ ($> Q_c \simeq 17.0$), showing a solution on the upper branch, with $h_m = 3.3289$. Note that in this figure the streamlines are not plotted at equal intervals in ψ. The curve $z = \frac{2}{3}h$ (which the streamlines cross 'vertically') is also shown.

the above asymptotic results, are also shown (as the dashed curves); the agreement is seen to be very good in both cases. Figure 11(c) is for the case $M = -1$ and $Q = 0.01$; in this case the free surface is essentially flat except in a boundary layer near $y = a$, and the transverse flow is confined to the boundary layer.

Figure 12 gives examples of the streamline patterns in the case $M = -0.5$ and $Q = 14$ ($< Q_c \simeq 17.0$); it is seen how, even though the free-surface profile is qualitatively the same in all cases, the flow changes rather rapidly with α, from a case at $\alpha = 2.181$ with a single eddy near the right of the rivulet, through a case at $\alpha = 2.182$ with two 'internal' eddies, to one at $\alpha = 2.1842$ with a single eddy considerably nearer to the centre of the rivulet. Since $Q < Q_c$ in figure 12, such a succession of transverse flows could occur in flow of a continuous rivulet round a large cylinder. Specifically, for sufficiently small α there is only one stagnation point, but as α increases through a critical value (lying in $\frac{1}{2}\pi < \alpha < \cos^{-1}(-255M^2/96) \simeq 2.297$) a pair of stagnation points is 'born', giving three in total; then as α increases through a second (larger) critical value two of these stagnation points coalesce and 'annihilate' each other, leaving just one.

Figure 13 gives an example of the streamline pattern in a case with $Q > Q_c$, namely $\alpha = 2.072$, $M = -0.5$ and $Q = 70$ ($> Q_c \simeq 17.0$). The figure shows a solution on the upper branch, with $h_m = 3.3289$; there is a very similar solution on the middle branch, with $h_m = 3.2088$. In both cases there are three stagnation points in $0 < y < a$, with two 'internal' eddies. In addition there is a solution on the lower branch with a single stagnation point in $0 < y < a$. Again it is unlikely that the middle-branch solution is realizable in practice.

5. Conclusions

We have used the lubrication approximation to investigate the steady flow of a thin rivulet of viscous fluid with prescribed volume flux draining down a planar or slowly varying substrate that is either uniformly hotter or uniformly colder than the

https://doi.org/10.1017/S0022112001004797 Published online by Cambridge University Press

surrounding atmosphere, when the surface tension of the fluid varies linearly with temperature. Utilizing the (implicit) solution of the governing ordinary differential equation that emerges, we undertook a comprehensive asymptotic and numerical analysis of the flow, including a detailed description of the different forms that the cross-sectional profile of the rivulet may take. In particular, it was shown that the variation in surface tension drives a transverse flow that causes the fluid particles to spiral down the rivulet in helical vortices. In general the transverse flow in $0 < y < a$ has either one stagnation point (around which all the fluid circulates) or three stagnation points (with two 'internal' eddies surrounded by circulating fluid). Also it was found that a single continuous rivulet can run from the top to the bottom of a large horizontal circular cylinder provided that the cylinder is either warmer ($M > 0$) or significantly cooler ($M \leqslant -\frac{2}{3}$) than the surrounding atmosphere, but if it is only slightly cooler ($-\frac{2}{3} < M < 0$) then a continuous rivulet is possible only for a sufficiently small flux ($Q \leqslant Q_c$), though a rivulet with a discontinuity in the free surface is possible for larger values of the flux ($Q > Q_c$). Moreover, near the top of the cylinder the rivulet has finite depth but infinite width, whereas near the bottom of the cylinder it has finite width and infinite depth if the cylinder is heated or slightly cooled ($M > -\frac{2}{3}$), but has infinite width and finite depth if the cylinder is significantly cooled ($M \leqslant -\frac{2}{3}$). In practice such marked differences in the width and depth of the rivulet could dramatically affect the transfer of heat between the substrate and the atmosphere.

The first author (D.H.) wishes to thank the Engineering and Physical Sciences Research Council for financial support via a studentship during the course of the present work.

Appendix A. The form of the free-surface profile $h(y)$

In this appendix we prove that the rivulet profile $h(y)$ has a single stationary point, a maximum at $y = 0$. The proof given here (which is shorter and more elegant than the authors' original proof) is due to Professor J. B. McLeod (University of Pittsburgh).

The function $h(y)$ satisfies the differential equation (36), namely

$$(h_{yy} - h\cos\alpha)_y + \frac{3Mh_y}{2h(1+Bh)^2} = 0, \tag{A 1}$$

with

$$h_y(0) = 0, \quad h(a) = 0, \quad h_y(a) = -1, \tag{A 2}$$

and $h \geqslant 0$; also we define h_m by $h_m = h(0)$. (Note that at this stage h_m is not necessarily the global maximum of $h(y)$ in $-a \leqslant y \leqslant a$.) Let $y = y_0$ ($0 \leqslant y_0 < a$) be the position of the stationary point of $h(y)$ that is nearest to $y = a$. Define the functions $h_1(\xi)$ and $h_2(\xi)$ by $h_1(\xi) = h(y_0 + \xi)$ and $h_2(\xi) = h(y_0 - \xi)$. Then the $h_k(\xi)$ ($k = 1, 2$) satisfy

$$(h_{k\xi\xi} - h_k\cos\alpha)_\xi + \frac{3Mh_{k\xi}}{2h_k(1+Bh_k)^2} = 0, \tag{A 3}$$

$$h_1(0) = h_2(0), \quad h_{1\xi}(0) = h_{2\xi}(0) = 0, \quad h_{1\xi\xi}(0) = h_{2\xi\xi}(0). \tag{A 4}$$

The uniqueness of the solution of such an initial-value problem (at least up to the singularity at $y = a$, where $h = 0$) means that $h_1(\xi) = h_2(\xi)$. Thus $h(y_0+\xi) = h(y_0-\xi)$, that is, h is symmetric about the stationary point $y = y_0$, which must therefore be the unique maximum h_m of $h(y)$ in $-a \leqslant y \leqslant a$, at $y = y_0 = 0$.

https://doi.org/10.1017/S0022112001004797 Published online by Cambridge University Press

Appendix B. The solution in the limit $M \to 0$

Here we obtain the asymptotic form of the solution $h(y)$ to $O(M)$ in the limit $M \to 0$. We achieve this by substituting the expansions (71) into the differential equation (37), the boundary conditions (13*a*) at $y = 0$ and (26) at $y = a$, and the flux condition (34), and solving the problem that emerges at each order in M. At leading order this yields the third-order differential equation

$$(h_{0yy} - h_0 \cos\alpha)_y = 0, \tag{B 1}$$

to be integrated subject to the boundary conditions

$$h_{0y}(0) = 0, \quad h_0(a_0) = 0, \quad h_{0y}(a_0) = -1. \tag{B 2}$$

Hence h_0 and a_0 are the solutions of the isothermal problem studied by Duffy & Moffatt (1995), namely

$$h_0(y) = \begin{cases} \dfrac{\cosh Ga_0 - \cosh Gy}{G \sinh Ga_0} & \text{if} \quad 0 \leqslant \alpha < \tfrac{1}{2}\pi, \\ \dfrac{a_0^2 - y^2}{2a_0} & \text{if} \quad \alpha = \tfrac{1}{2}\pi, \\ \dfrac{\cos Gy - \cos Ga_0}{G \sin Ga_0} & \text{if} \quad \tfrac{1}{2}\pi < \alpha \leqslant \pi, \end{cases} \tag{B 3}$$

where again $G = |\cos\alpha|^{1/2}$, and a_0 is obtained from (34) as the solution of

$$Q = \begin{cases} \dfrac{\sin\alpha}{9G^4}\left(15Ga_0 \coth^3 Ga_0 - 15\coth^2 Ga_0 - 9Ga_0 \coth Ga_0 + 4\right) & \text{if} \quad 0 \leqslant \alpha < \tfrac{1}{2}\pi, \\ \dfrac{4a_0^4}{105} & \text{if} \quad \alpha = \tfrac{1}{2}\pi, \\ \dfrac{\sin\alpha}{9G^4}\left(-15Ga_0 \cot^3 Ga_0 + 15\cot^2 Ga_0 - 9Ga_0 \cot Ga_0 + 4\right) & \text{if} \quad \tfrac{1}{2}\pi < \alpha \leqslant \pi \end{cases} \tag{B 4}$$

(with h_{m0} found by setting $y = 0$ in h_0). At first order in M equation (37) yields

$$(h_{1yy} - h_1 \cos\alpha)_y + \frac{3h_{0y}}{2h_0} = 0, \tag{B 5}$$

to be integrated subject to the boundary conditions

$$h_{1y}(0) = 0, \quad h_1(a_0) + a_1 h_{0y}(a_0) = 0, \quad h_{1y}(a_0) + a_1 h_{0yy}(a_0) = 0, \tag{B 6}$$

together with the first-order flux condition

$$\int_0^{a_0} h_0^2 h_1 \, \mathrm{d}y = 0. \tag{B 7}$$

We thus obtain (after considerable algebra)

$$h_1 = a_1(1 - Gh_0 \coth Ga_0) + \frac{3}{2G^2}\left[Gy \sinh Gy \cosh Ga_0 \right. \\ \left. + (s_+ + s_-)(2\log(\sinh Ga_0) - Ga_0 \coth Ga_0) - s_+ \log s_+ - s_- \log s_-\right], \tag{B 8}$$

$$a_1 = -\frac{3}{4G^2}\left[\frac{13\coth Ga_0 + (17\coth^2 Ga_0 - 5)Ga_0 - 6I(5\coth^2 Ga_0 - 1)}{15\coth^3 Ga_0 - 13\coth Ga_0 - 3Ga_0(5\coth^2 Ga_0 - 1)\operatorname{cosech}^2 Ga_0}\right] \tag{B 9}$$

https://doi.org/10.1017/S0022112001004797 Published online by Cambridge University Press

for $0 \leqslant \alpha < \frac{1}{2}\pi$, where $s_{\pm} = \sinh^2[\frac{1}{2}G(a_0 \pm y)]$ and $I = I(Ga_0)$ is given by

$$I = \int_0^{Ga_0} \xi^2 \operatorname{cosech}^2 \xi \, \mathrm{d}\xi. \tag{B 10}$$

At $\alpha = \frac{1}{2}\pi$ we have

$$h_1 = \frac{a_1(a_0^2 + y^2)}{2a_0^2} + \tfrac{3}{4}\left[2(a_0^2 + y^2)\log(2a_0) - (a_0^2 - y^2)\right.$$
$$\left. -(a_0 + y)^2 \log(a_0 + y) - (a_0 - y)^2 \log(a_0 - y)\right], \tag{B 11}$$

$$a_1 = -\frac{113a_0^2}{280}, \tag{B 12}$$

which may be obtained by letting $G \to 0$ in (B 8)–(B 10); moreover h_1 and a_1 for $\frac{1}{2}\pi < \alpha \leqslant \pi$ may be obtained by replacing G by iG in (B 8)–(B 10). In each case h_{m1} is obtained by setting $y = 0$ in h_1.

REFERENCES

Alekseenko, S. V., Geshev, P. I. & Kuibin, P. A. 1997 Free-boundary fluid flow on an inclined cylinder. *Phys. Dokl.* **42**, 269–272.

Allen, R. F. & Biggin, C. M. 1974 Longitudinal flow of a lenticular liquid filament down an inclined plane. *Phys. Fluids* **17**, 287–291.

Anderson, D. M. & Davis, S. H. 1995 The spreading of volatile liquid droplets on heated surfaces. *Phys. Fluids* **7**, 248–265.

Braun, R. J., Murray, B. T., Boettinger, W. J. & McFadden, G. B. 1995 Lubrication theory for reactive spreading of a thin drop. *Phys. Fluids* **7**, 1797–1810.

Burelbach, J. P., Bankoff, S. G. & Davis, S. H. 1988 Nonlinear stability of evaporating/condensing liquid films. *J. Fluid Mech.* **195**, 463–494.

Burelbach, J. P., Bankoff, S. G. & Davis, S. H. 1990 Steady thermocapillary flows of thin liquid layers. II. Experiment. *Phys. Fluids* A **2**, 322–333.

Davis, S. H. 1980 Moving contact lines and rivulet instabilities. Part 1. The static rivulet. *J. Fluid Mech.* **98**, 225–242.

Davis, S. H. 1987 Thermocapillary instabilities. *Ann. Rev. Fluid Mech.* **19**, 403–435.

Duffy, B. R. & Moffatt, H. K. 1995 Flow of a viscous trickle on a slowly varying incline. *Chem. Engng J.* **60**, 141–146.

Duffy, B. R. & Moffatt, H. K. 1997 A similarity solution for viscous source flow on a vertical plane. *Euro. J. Appl. Maths* **8**, 37–47.

Ehrhard, P. 1993 Experiments on isothermal and non-isothermal spreading. *J. Fluid Mech.* **257**, 463–483.

Ehrhard, P. & Davis, S. H. 1991 Non-isothermal spreading of liquid drops on horizontal plates. *J. Fluid Mech.* **229**, 365–388.

Hartley, D. E. & Murgatroyd, W. 1964 Criteria for the break-up of thin liquid layers flowing isothermally over solid surfaces. *Intl J. Heat Mass Transfer* **7**, 1003–1015.

Hinch, E. J. 1991 *Perturbation Methods.* Cambridge University Press.

Jensen, O. E. & Grotberg, J. B. 1993 The spreading of heat or soluble surfactant along a thin liquid film. *Phys. Fluids* A **5**, 58–68.

Joo, S. W., Davis, S. H. & Bankoff, S. G. 1996 A mechanism for rivulet formation in heated falling films. *J. Fluid Mech.* **321**, 279–298.

Kataoka, D. E. & Troian, S. M. 1997 A theoretical study of instabilities at the advancing front of thermally driven coating films. *J. Colloid Interface Sci.* **192**, 350–362.

Kataoka, D. E. & Troian, S. M. 1998 Stabilising the advancing front of thermally driven climbing films. *J. Colloid Interface Sci.* **203**, 335–344.

https://doi.org/10.1017/S0022112001004797 Published online by Cambridge University Press

KUIBIN, P. A. 1996 An asymptotic description of the rivulet flow along an inclined cylinder. *Russ. J. Engng Thermophys.* **6**, 33–45.

LÓPEZ, P. G., BANKOFF, S. G. & MIKSIS, M. J. 1996 Non-isothermal spreading of a thin liquid film on an inclined plane. *J. Fluid Mech.* **324**, 261–286.

ORON, A., DAVIS, S. H. & BANKOFF, S. G. 1997 Long-scale evolution of thin liquid films. *Rev. Mod. Phys.* **69**, 931–980.

PODGORSKI, T., FLESSELLES, J.-M. & LIMAT, L. 1999 Dry arches within flowing films. *Phys. Fluids* **11**, 845–852.

PONTER, A. B., DAVIES, G. A., ROSS, T. K. & THORNLEY, P. G. 1967 The influence of mass transfer on liquid film breakdown. *Intl J. Heat Mass Transfer* **10**, 349–359.

REISFELD, B. & BANKOFF, S. G. 1992 Non-isothermal flow of a liquid film on a horizontal cylinder. *J. Fluid Mech.* **236**, 167–196.

ROSENBLAT, S. 1983 Rivulet flow of a viscoelastic liquid. *J. Non-Newtonian Fluid Mech.* **13**, 259–277.

SCHMUKI, P. & LASO, M. 1990 On the stability of rivulet flow. *J. Fluid Mech.* **215**, 125–143.

SMITH, M. K. 1995 Thermocapillary migration of a two-dimensional liquid droplet on a solid surface. *J. Fluid Mech.* **294**, 209–230.

SMITH, P. C. 1973 A similarity solution for slow viscous flow down an inclined plane. *J. Fluid Mech.* **58**, 275–288.

TAN, M. J., BANKOFF, S. G. & DAVIS, S. H. 1990 Steady thermocapillary flows of thin liquid layers. I. Theory. *Phys. Fluids* A **2**, 313–321.

TOWELL, G. D. & ROTHFELD, L. B. 1966 Hydrodynamics of rivulet flow. *AIChE J.* **12**, 972–980.

WEILAND, R. H. & DAVIS, S. H. 1981 Moving contact lines and rivulet instabilities. Part 2. Long waves on flat rivulets. *J. Fluid Mech.* **107**, 261–280.

WILSON, S. D. R. 1974 The stability of a dry patch on a wetted wall. *Intl J. Heat Mass Transfer* **17**, 1607–1615.

WILSON, S. K. & DUFFY, B. R. 1998 On the gravity-driven draining of a rivulet of viscous fluid down a slowly varying substrate with variation transverse to the direction of flow. *Phys. Fluids* **10**, 13–22.

WILSON, S. K., DUFFY, B. R. & DAVIS, S. H. 2001 On a slender dry patch in a liquid film draining under gravity down an inclined plane. *Eur. J. Appl. Maths* (to appear).

YOUNG, G. W. & DAVIS, S. H. 1987 Rivulet instabilities. *J. Fluid Mech.* **176**, 1–31.

https://doi.org/10.1017/S0022112001004797 Published online by Cambridge University Press